Vitamin B_{12}–dependent taurine synthesis regulates growth and bone mass

Pablo Roman-Garcia,[1] Isabel Quiros-Gonzalez,[1] Lynda Mottram,[2,3] Liesbet Lieben,[1,2] Kunal Sharan,[1,2] Arporn Wangwiwatsin,[1] Jose Tubio,[4] Kirsty Lewis,[1,2] Debbie Wilkinson,[5] Balaji Santhanam,[1,6] Nazan Sarper,[7] Simon Clare,[3] George S. Vassiliou,[4] Vidya R. Velagapudi,[8] Gordon Dougan,[3] and Vijay K. Yadav[1,2]

[1]Systems Biology of Bone Laboratory, [2]Sanger Mouse Genetics Project, Department of Mouse and Zebrafish Genetics, [3]Department of Pathogen Genetics, and [4]Department of Human Genetics, Wellcome Trust Sanger Institute, Cambridge, United Kingdom. [5]Instrument Core Facility, University of Aberdeen, Foresterhill, Aberdeen, United Kingdom. [6]Laboratory of Molecular Biology, Medical Research Council, Cambridge, United Kingdom. [7]Pediatrics and Pediatric Hematology, Kocaeli University Hospital, Kocaeli, Turkey. [8]Metabolomics Unit, Institute for Molecular Medicine Finland FIMM, Helsinki, Finland.

Both maternal and offspring-derived factors contribute to lifelong growth and bone mass accrual, although the specific role of maternal deficiencies in the growth and bone mass of offspring is poorly understood. In the present study, we have shown that vitamin B_{12} (B_{12}) deficiency in a murine genetic model results in severe postweaning growth retardation and osteoporosis, and the severity and time of onset of this phenotype in the offspring depends on the maternal genotype. Using integrated physiological and metabolomic analysis, we determined that B_{12} deficiency in the offspring decreases liver taurine production and associates with abrogation of a growth hormone/insulin-like growth factor 1 (GH/IGF1) axis. Taurine increased GH-dependent IGF1 synthesis in the liver, which subsequently enhanced osteoblast function, and in B_{12}-deficient offspring, oral administration of taurine rescued their growth retardation and osteoporosis phenotypes. These results identify B_{12} as an essential vitamin that positively regulates postweaning growth and bone formation through taurine synthesis and suggests potential therapies to increase bone mass.

Introduction

The maternal environment plays a fundamental role in the development of the fetus in utero and during postnatal life (1, 2). Factors derived from the mother and transported through the placenta, including nutrients and hormones, regulate many physiological processes in the fetus and thus greatly influence late-life health of the offspring (3). During late gestation and the early postnatal period, there is an exponential deposition of bone in animals, known as bone accrual, that determines the peak bone mass achieved in the adult skeleton (4). The process that regulates bone accrual, also known as remodeling, consists of 2 phases: resorption of preexisting mineralized bone matrix by the osteoclast, followed by de novo bone formation by the osteoblast (5–9). Despite the importance of the maternal environment in this process, the mechanisms through which maternally derived factors regulate neonatal growth and bone mass are still poorly understood.

In humans, vitamin B_{12} (B_{12}) deficiency is associated with growth retardation, reduced serum osteocalcin levels, lower bone mineral density, and increased bone fracture risk, yet the underlying mechanisms remain unclear (10–16). B_{12} is an essential water-soluble vitamin that regulates a multitude of cellular processes in vertebrates (17). In cells, B_{12} derivatives function as cofactors for only 2 known enzymes, methionine synthase (MTR) and methylmalonyl-CoA mutase (MUT), and through them affect a variety of downstream metabolic pathways, such as Kreb's cycle, amino acid synthesis, and DNA and histone methylation (18). Mammals can recycle B_{12} to maintain cellular processes dependent on B_{12} (19). Absorption of dietary B_{12} requires gastric intrinsic factor (Gif), a stomach-specific protein that is essential for the absorption of B_{12} from the gut lumen into the bloodstream (17), which is then stored in the liver. A decrease in the production of functional Gif protein therefore causes B_{12} deficiency.

Activation of the hypothalamic/pituitary growth hormone (GH) axis during the early postweaning period in the offspring determines the longitudinal and cross-sectional expansion of the skeleton and other organs in vertebrates (20–22). Perturbations in GH action during early independent life of the offspring result in multiple abnormalities that manifest in skeleton and other organs (23–26). Over the last 20 years, mouse and human molecular genetic studies have identified numerous components in the GH axis that regulate the peripubertal growth spurt (23, 27). However, factors regulated by GH in the liver (by which it mediates its actions) are only now beginning to be understood.

Taurine, a sulfur-containing amino acid, is synthesized primarily by liver in the periphery, and after secretion in the circulation, it is accumulated in different tissues of the body (28). Although taurine is not incorporated in proteins, it is a (semi)essential amino acid for mammals that affects growth and metabolism (29). Consistent with the critical role of taurine in regulation of growth, its deficiency is often associated with prenatal and postnatal growth retardation (29). Despite the importance of taurine in regulating various biological functions, its interaction with the GH axis in the regulation of growth and bone metabolism remains undefined.

In the present study, we created a mouse genetic model of B_{12} deficiency by deleting the gene essential for B_{12} absorption from the gut, *Gif*, to understand the importance of maternally and offspring-derived B_{12} in the regulation of growth and bone mass homeostasis. Through mouse genetic and pharmacological assays using B_{12}-deficient offspring, we showed that maternally derived B_{12} is an essential nutrient that regulates taurine production in the offspring to regulate growth and bone mass. Importantly,

Authorship note: Pablo Roman-Garcia, Isabel Quiros-Gonzalez, and Lynda Mottram contributed equally to this work.

Conflict of interest: The authors have declared that no conflict of interest exists.

Citation for this article: *J Clin Invest.* 2014;124(7):2988–3002. doi:10.1172/JCI72606.

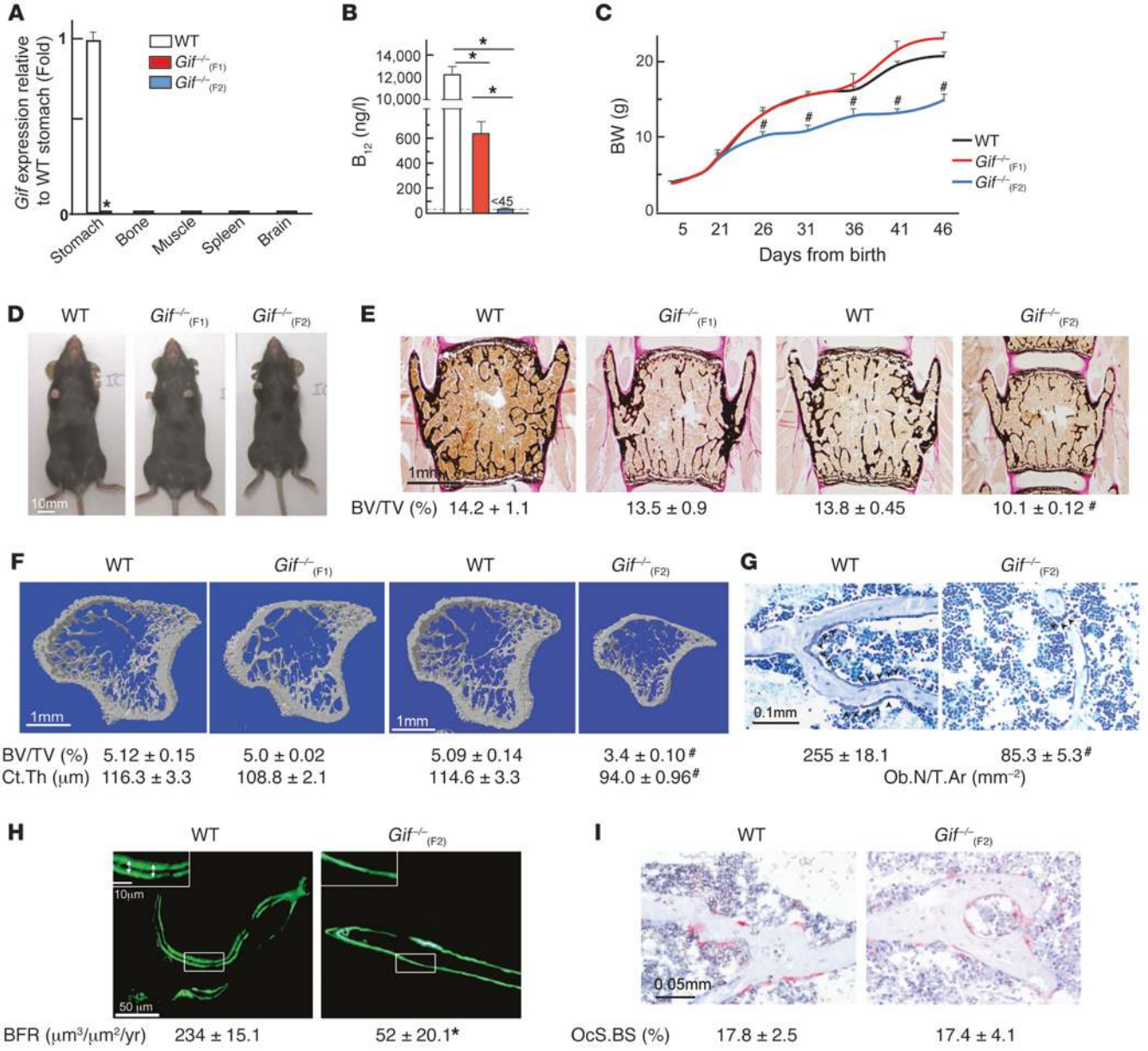

Figure 1

B_{12} deficiency in mice causes growth retardation and low bone mass. (**A**) Real-time PCR analysis of *Gif* expression in WT and *Gif*$^{-/-}$ tissues. (**B**) Serum B_{12} levels in WT, *Gif*$^{-/-}$$_{(F1)}$, and *Gif*$^{-/-}$$_{(F2)}$ mice. (**C**) BW analysis of WT, *Gif*$^{-/-}$$_{(F1)}$ and *Gif*$^{-/-}$$_{(F2)}$ mice. (**D**) Morphological analysis of 8-week-old WT, *Gif*$^{-/-}$$_{(F1)}$, and *Gif*$^{-/-}$$_{(F2)}$ mice. (**E** and **F**) Histological analysis of vertebrae (**E**) and μCT analysis of long bone (**F**) of WT, *Gif*$^{-/-}$$_{(F1)}$, and *Gif*$^{-/-}$$_{(F2)}$ mice. Mineralized bone matrix (black) was stained by von Kossa reagent. BV/TV, bone volume relative to total volume. Ct.Th., cortical thickness. (**G**) Toluidine blue staining showing reduced osteoblast number on bone surface, with quantification of Ob.N/T.Ar. (**H**) Photomicrographs showing near-absence of calcein double labeling on the surface of trabecular bone in *Gif*$^{-/-}$$_{(F2)}$ mice, with quantification of BFR. (**I**) Photomicrographs showing TRAP-stained osteoclasts on the bone surface (pink), with quantification of osteoclast surface per bone surface (OcS/BS). $^{\#}P < 0.05$; $^{*}P < 0.01$. Values are mean ± SEM. $n = 8$ [WT and *Gif*$^{-/-}$$_{(F2)}$]; 9 [*Gif*$^{-/-}$$_{(F2)}$]. Arrowheads on images indicate the location of cell types or parameters measured. Scale bars: 10 mm (**D**); 1 mm (**E** and **F**); 0.1 mm (**G**); 50 μm (**H**); 10 μm (**H**, insets); 0.05 mm (**I**). See also Supplemental Figure 1.

daily oral administration of taurine in B_{12}-deficient offspring was sufficient to prevent their growth defect and osteoporosis through normalization of the GH/IGF1 axis. These results identify B_{12} as an essential vitamin that regulates growth and bone mass and identify novel avenues to treat bone diseases associated with low bone formation.

Results

B_{12} deficiency causes growth retardation and low bone mass. To generate B_{12}-deficient animals, we first crossed *Gif*$^{+/-}$ female mice with *Gif*$^{+/-}$ male mice, yielding first-generation *Gif*$^{+/+}$ [*Gif*$^{+/+}$$_{(F1)}$] and *Gif*$^{-/-}$$_{(F1)}$ mice. Real-time PCR analysis of *Gif* expression across different tissues showed that *Gif* expression was restricted to the stomach

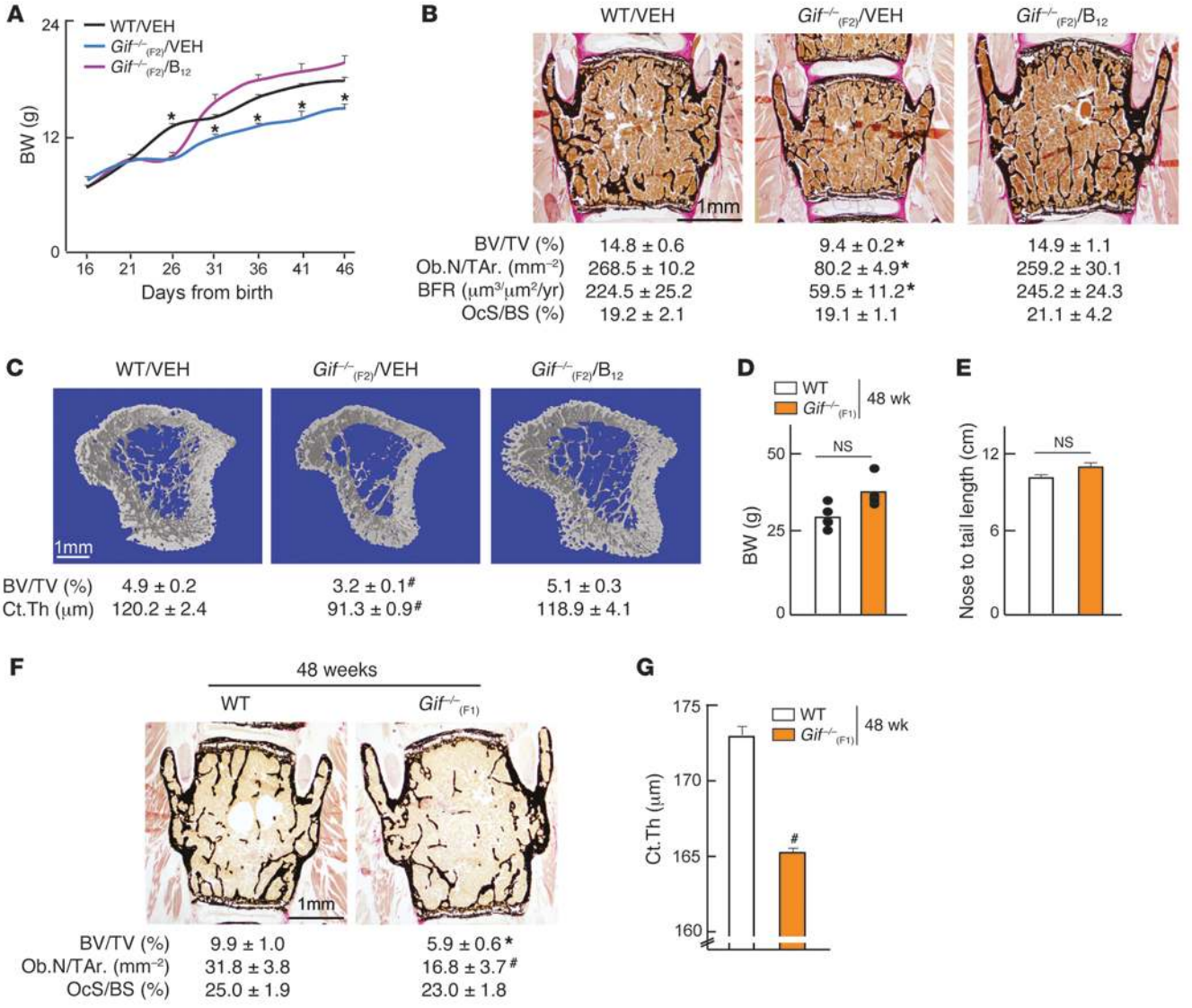

Figure 2

Maternal B_{12} regulates offspring growth and bone mass and B_{12} deficiency during aging regulates bone mass independently of body growth. (**A**) Growth curve analysis of WT/VEH, *Gif*$^{-/-}_{(F2)}$/VEH, and *Gif*$^{-/-}_{(F2)}$/B_{12} mice. (**B** and **C**) Histological analysis of vertebral bone (**B**) and μCT analysis of long bone (**C**) in 8-week-old WT/VEH, *Gif*$^{-/-}_{(F2)}$/VEH, and *Gif*$^{-/-}_{(F2)}$/B_{12} mice, with quantification of BV/TV, Ob.N/T.Ar., BFR, OcS/BS, and Ct.Th. (**D** and **E**) BW (**D**) and nose-to-tail length (**E**) of 48-week-old WT and *Gif*$^{-/-}_{(F1)}$ mice. (**F** and **G**) Histological analysis of vertebral bone (**F**) and Ct.Th. analysis of long bone (**G**) in 48-week-old WT and *Gif*$^{-/-}_{(F1)}$ mice, with quantification of BV/TV, Ob.N/T.Ar., OcS/BS, and Ct.Th. $^{\#}P < 0.05$; $^{*}P < 0.01$. Values are mean ± SEM. n = 4–6 [WT]; 5 [*Gif*$^{-/-}_{(F2)}$/VEH], 7 [*Gif*$^{-/-}_{(F2)}$/B_{12}]; 6 [*Gif*$^{-/-}_{(F1)}$]. All mice shown are females. Scale bars: 1 mm (**B**, **C**, and **F**). See also Supplemental Figure 2.

of WT mice, and this was abolished in *Gif*$^{-/-}_{(F1)}$ mice (Figure 1A). Measurement of serum B_{12} levels in *Gif*$^{-/-}_{(F1)}$ offspring revealed a >20-fold reduction compared with WT mice (600 ± 35 versus 12,000 ± 110 ng/l), yet these mice still harbored detectable levels of serum B_{12} (Figure 1B). To further deplete B_{12} levels in the offspring, we next crossed *Gif*$^{-/-}_{(F1)}$ females with *Gif*$^{-/-}_{(F1)}$ males to generate second-generation *Gif*$^{-/-}_{(F2)}$ mice; WT control mice were generated by crossing *Gif*$^{+/+}_{(F1)}$ females with *Gif*$^{+/+}_{(F1)}$ males. Measurement of serum B_{12} revealed low levels of <45 ng/l (i.e., below the limit of detection of the assay) in *Gif*$^{-/-}_{(F2)}$ mice, compared with >11,000 ng/l in WT mice (Figure 1B). These results revealed that lowered B_{12} levels in *Gif*$^{-/-}_{(F1)}$ females resulted in inadequate B_{12} transfer to their progeny during pregnancy, which led to very low levels of B_{12} in their serum.

We used *Gif*$^{-/-}_{(F1)}$ and *Gif*$^{-/-}_{(F2)}$ mice to address the effect of altered B_{12} levels on postnatal growth and bone mass accrual. There was no major difference in the growth of WT, *Gif*$^{-/-}_{(F1)}$, and *Gif*$^{-/-}_{(F2)}$ animals until P21 (Figure 1C and Supplemental Figure 1, A and B; supplemental material available online with this article; doi:10.1172/JCI72606DS1). However, *Gif*$^{-/-}_{(F2)}$ animals showed growth arrest between P21 and P26, as evidenced by their impaired BW gain and reduced body size compared with WT, *Gif*$^{-/-}_{(F1)}$, and *Gif*$^{+/-}_{(F2)}$ animals (Figure 1, C and D, and Supplemental Figure 1C). These results indicated that although *Gif*$^{-/-}_{(F2)}$ mice have normal early

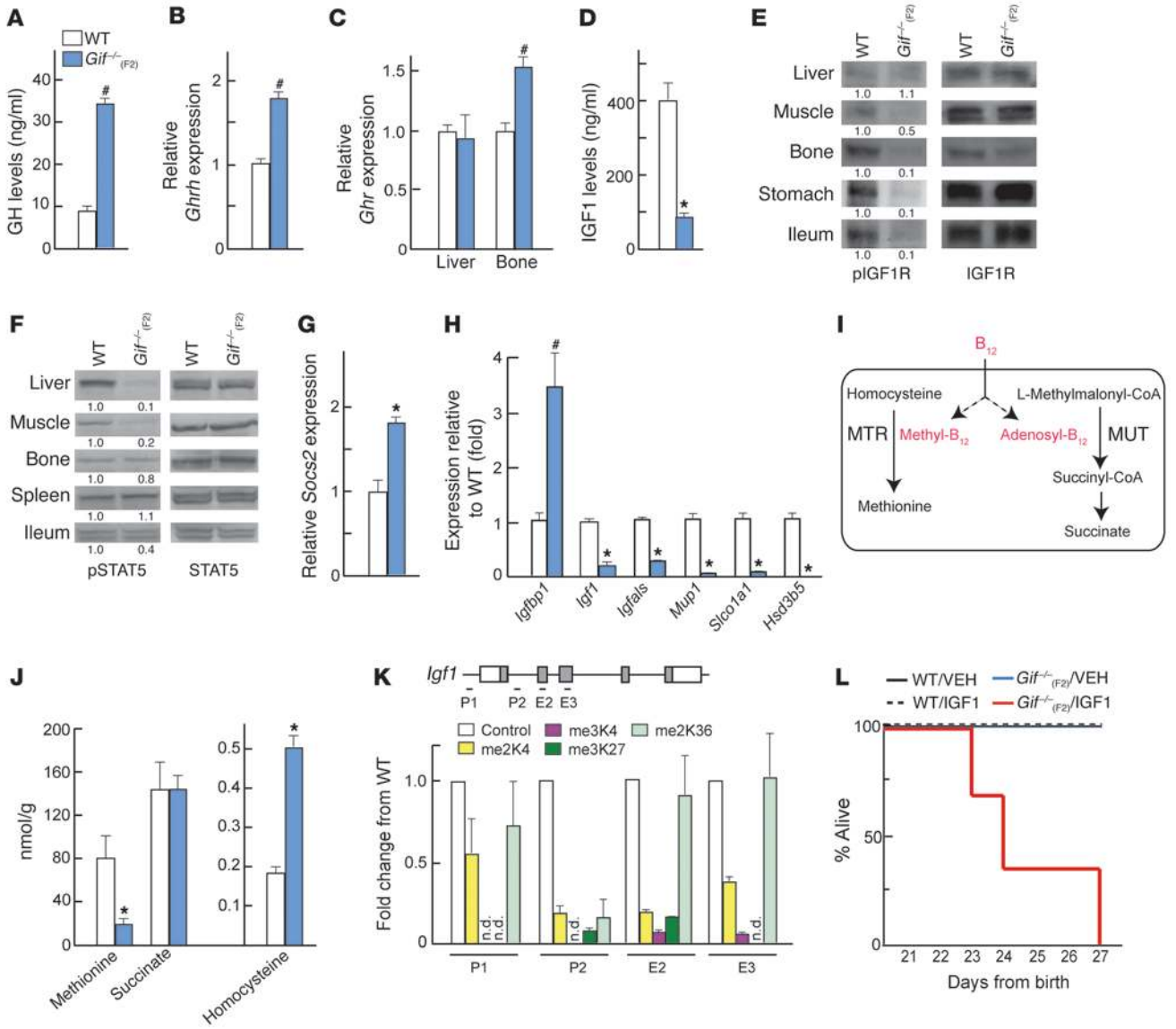

Figure 3

B_{12} deficiency causes GH resistance. (**A**) Serum GH levels in WT (n = 6) and *Gif*$^{-/-}$$_{(F2)}$ (n = 5) mice. (**B** and **C**) Real-time PCR analysis of *Ghrh* in the hypothalamus (Hyp) (**B**), and *Ghr* expression in liver and bone (**C**), of WT and *Gif*$^{-/-}$$_{(F2)}$ mice (n = 5 per group). (**D**) Serum IGF1 levels in WT and *Gif*$^{-/-}$$_{(F2)}$ mice (n = 7–10). (**E** and **F**) Western blot analysis of IGF1R (**E**) and STAT5 (**F**) phosphorylation in different WT and *Gif*$^{-/-}$$_{(F2)}$ tissues; blotting was done on the same blot after stripping the membrane for pIGF1R and pSTAT5, respectively. A representative blot from 3 independent experiments is shown; different tissues were run noncontiguously. Relative quantification of pIGF1R and pSTAT5 (normalized to IGF1R and STAT5, respectively) is shown below. (**G** and **H**) Real-time PCR analysis of *Socs2* (**G**) and STAT5 target gene (**H**) expression in WT and *Gif*$^{-/-}$$_{(F2)}$ liver (n = 5 per group). (**I**) Enzymatic reactions of MTR and MUT dependent on the B_{12}-generated cofactors methyl-B_{12} and adenosyl-B_{12}, respectively. (**J**) Levels of methionine, succinate, and homocysteine (nmol/g liver tissue) in WT and *Gif*$^{-/-}$$_{(F2)}$ mice (n = 5 per group). (**K**) ChIP analysis of methylated histones, shown relative to control (assigned as 1), in different regions of *Igf1* in *Gif*$^{-/-}$$_{(F2)}$ liver. P-, promoter; E-, exon; n.d., not detectable. (**L**) Survival of WT/VEH, WT/IGF1, *Gif*$^{-/-}$$_{(F2)}$/VEH, and *Gif*$^{-/-}$$_{(F2)}$/IGF1 mice ($n$ = 5 per group). $^{\#}P < 0.05$; $^{*}P < 0.01$. Values are mean ± SEM. See also Supplemental Figure 3.

postnatal development, the postweaning growth spurt observed in WT animals is severely compromised in these mice.

Histological and μCT analyses in 8-week-old WT, *Gif*$^{-/-}$$_{(F1)}$, and *Gif*$^{-/-}$$_{(F2)}$ mice revealed a severe decrease in bone mass in vertebra and long bone in *Gif*$^{-/-}$$_{(F2)}$ animals, whereas levels were similar between *Gif*$^{-/-}$$_{(F1)}$ and WT mice (Figure 1, E and F). The low bone mass in *Gif*$^{-/-}$$_{(F2)}$ mice was caused by a >3-fold decrease in number of osteoblasts per trabecular area (Ob.N/T.Ar.), with a dramatic decrease in bone formation rate (BFR), compared with WT mice (Figure 1, G and H). In contrast to the deleterious consequences of B_{12} deficiency on osteoblast number and function, osteoclast parameters in *Gif*$^{-/-}$$_{(F2)}$ mice were similar to those of WT mice (Figure 1I).

Together, these results obtained in first- and second-generation *Gif*$^{-/-}$ offspring showed (a) that maternally derived B_{12} is trans-

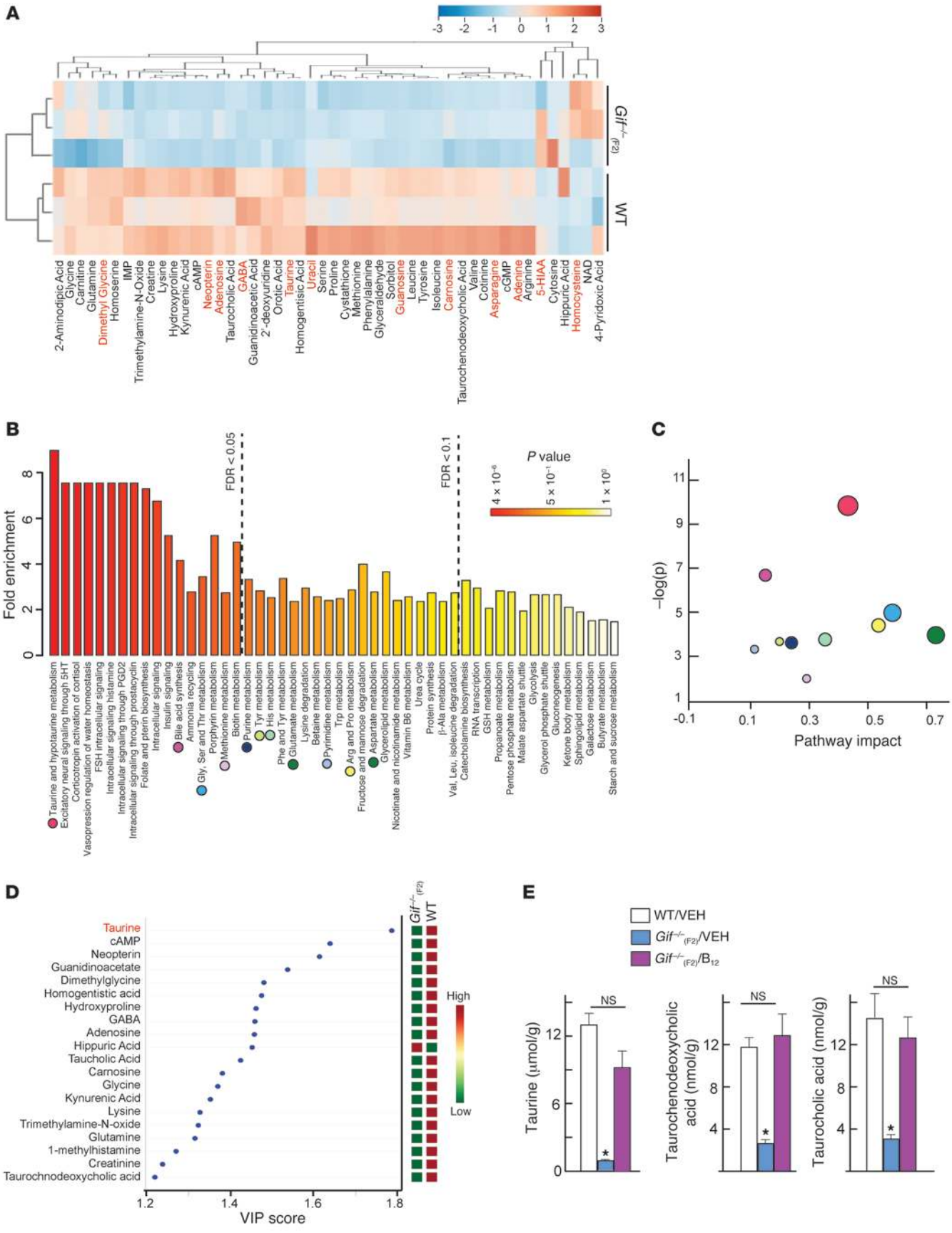
A
-3 -2 -1 0 1 2 3
Gif−/− (F2)
WT
2-Aminodipic Acid
Glycine
Carnitine
Glutamine
Dimethyl Glycine
Homoserine
IMP
Trimethylamine-N-Oxide
Creatine
Lysine
Hydroxyproline
Kynurenic Acid
cAMP
Neopterin
Adenosine
Taurocholic Acid
GABA
Guanidinoacetic Acid
2'-deoxyuridine
Orotic Acid
Taurine
Homogentisic Acid
Uracil
Serine
Proline
Cystathione
Methionine
Phenylalanine
Glyceraldehyde
Sorbitol
Guanosine
Leucine
Tyrosine
Isoleucine
Carnosine
Taurochenodeoxycholic Acid
Valine
Cotinine
Asparagine
cGMP
Adenine
Arginine
5-HIAA
Cytosine
Hippuric Acid
Homocysteine
NAD
4-Pyridoxic Acid
B
Fold enrichment
FDR < 0.05
FDR < 0.1
P value
4 × 10−6
5 × 10−1
1 × 100
Taurine and hypotaurine metabolism
Excitatory neural signaling through 5HT
Corticotropin activation of cortisol
Vasopressin regulation of water homeostasis
FSH intracellular signaling
Intracellular signaling histamine
Intracellular signaling through PGD2
Intracellular signaling through prostacyclin
Folate and pterin biosynthesis
Intracellular signaling
Insulin signaling
Bile acid synthesis
Ammonia recycling
Gly, Ser and Thr metabolism
Porphyrin metabolism
Methionine metabolism
Biotin metabolism
Purine metabolism
Tyr metabolism
His metabolism
Phe and Tyr metabolism
Glutamate metabolism
Lysine degradation
Betaine metabolism
Pyrimidine metabolism
Trp metabolism
Arg and Pro metabolism
Fructose and mannose degradation
Aspartate metabolism
Glycerolipid metabolism
Nicotinate and nicotinamide metabolism
Vitamin B6 metabolism
Urea cycle
Protein synthesis
β-Ala metabolism
Val, Leu, isoleucine degradation
Catecholamine biosynthesis
RNA transcription
GSH metabolism
Propanoate metabolism
Pentose phosphate metabolism
Malate aspartate shuttle
Glycolysis
Glycerol phosphate shuttle
Gluconeogenesis
Ketone body metabolism
Sphingolipid metabolism
Galactose metabolism
Butyrate metabolism
Starch and sucrose metabolism
C
−log(p)
Pathway impact
D
Taurine
cAMP
Neopterin
Guanidinoacetate
Dimethylglycine
Homogentistic acid
Hydroxyproline
GABA
Adenosine
Hippuric Acid
Taucholic Acid
Carnosine
Glycine
Kynurenic Acid
Lysine
Trimethylamine-N-oxide
Glutamine
1-methylhistamine
Creatinine
Taurochnodeoxycholic acid
Gif−/− (F2)
WT
High
Low
VIP score
E
WT/VEH
Gif−/− (F2)/VEH
Gif−/− (F2)/B12
Taurine (μmol/g)
Taurochenodeoxycholic acid (nmol/g)
Taurocholic acid (nmol/g)
NS
*

Figure 4
Metabolomics analysis identifies taurine as a critical metabolite that connects B_{12} deficiency with GH signaling. (**A**) Supervised hierarchical clustering plot of up- or downregulated metabolites in $Gif^{-/-}{}_{(F2)}$ liver. Metabolites regulated by GH in hepatocytes are shown in red font. (**B**) Summary plot for quantitative enrichment analysis. Metabolite sets are ranked according to false discovery rate (FDR); dashed lines show FDR value cutoffs. (**C**) Metabolome view reflects on the *x* axis increasing metabolic pathway impact according to the betweenness centrality measure, which shows key nodes in metabolic pathways that have been significantly altered upon B_{12} deficiency. Colored circles correspond to pathways in **B**. (**D**) PLSDA-VIP plot. Metabolites are ranked according to their increasing importance to group separation between WT and $Gif^{-/-}{}_{(F2)}$ mice. (**E**) Measurement of taurine and its derivatives in WT/VEH, $Gif^{-/-}{}_{(F2)}$/VEH, and $Gif^{-/-}{}_{(F2)}/B_{12}$ liver ($n = 5$ per group). $^{\#}P < 0.05$; $^{*}P < 0.01$. Values are mean ± SEM. See also Supplemental Figure 4.

ferred through at least 2 generations (in the first, it is sufficient to support offspring growth, but further depletion in the second fails to support their postweaning growth spurt) and (b) that B_{12} deficiency in the offspring decreases bone mass by reducing osteoblast numbers and bone formation without affecting bone resorption.

A single injection of B_{12} to the mothers prevents growth retardation and osteoporosis in $Gif^{-/-}{}_{(F2)}$ offspring. To address whether the growth retardation and osteoporosis in $Gif^{-/-}{}_{(F2)}$ progeny was due to the inability of their mothers to transfer adequate B_{12}, we next gave a single injection of B_{12} to $Gif^{-/-}{}_{(F1)}$ mothers. Pregnant WT and $Gif^{-/-}{}_{(F1)}$ females were given either vehicle or a single s.c. injection of 200 μg cyanocobalamin (CN-B_{12}) at 12.5 days post coitum (dpc), and their offspring [referred to herein as $Gif^{-/-}{}_{(F2)}$/VEH and $Gif^{-/-}{}_{(F2)}/B_{12}$, respectively] were studied. Growth curve analysis showed that although $Gif^{-/-}{}_{(F2)}/B_{12}$ offspring, like $Gif^{-/-}{}_{(F2)}$/VEH mice, showed growth retardation from P21 to P26, they rapidly caught up with WT mouse growth between P26 and P31, and were in fact indistinguishable from WT animals at P31 and thereafter (Figure 2A). In addition, bone histology and histomorphometry analysis at 8 weeks of age showed that the low bone mass observed in $Gif^{-/-}{}_{(F2)}$/VEH mice was completely prevented, in both vertebra and long bones, in $Gif^{-/-}{}_{(F2)}/B_{12}$ mice to levels seen in WT mice, due to the normalization of bone formation parameters (Figure 2, B and C). Growth curve and bone parameters were also normalized in male $Gif^{-/-}{}_{(F2)}/B_{12}$ mice to levels seen in WT mice (Supplemental Figure 2, A–I). Thus, a single s.c. injection of CN-B_{12} to $Gif^{-/-}{}_{(F1)}$ mothers was sufficient to rescue growth retardation and bone loss in their progeny at 8 weeks of age. Although $Gif^{-/-}{}_{(F2)}/B_{12}$ offspring had similar BW and bone mass at 8 weeks of age, they still displayed growth retardation during P21–P26, indicative of a higher requirement for B_{12} during this period. To test this contention, we next gave a single injection of B_{12} to the offspring on P11, closer to growth retardation onset at P21. This single injection to the offspring fully rescued their growth parameters up to 24 weeks of age (Supplemental Figure 2J and data not shown), which indicates that the exponential growth observed after weaning in offspring indeed requires a higher amount of B_{12}.

B_{12} deficiency during aging regulates bone mass independently of body growth. Our observation that the maternally derived pool of B_{12} in $Gif^{-/-}{}_{(F1)}$ mice was sufficient to support their postnatal growth and bone mass until adulthood provided us with a model wherein we can use aged F1 mice to dissociate the effect of maternal B_{12} on bone mass from its effect on growth. We reasoned that because $Gif^{-/-}{}_{(F1)}$ mice do not have the ability to absorb B_{12} from their diets and only receive a finite amount of B_{12} from their mothers, they would eventually deplete this store, become B_{12} deficient, and develop osteoporosis. Consistent with this model, analysis of 48-week-old $Gif^{-/-}{}_{(F1)}$ mice revealed normal growth, as evidenced by normal BW and nose-to-tail length, compared with WT mice (Figure 2, D and E). In contrast to their normal BW, 48-week-old $Gif^{-/-}{}_{(F1)}$ mice displayed a severe decrease in bone mass compared with WT animals in both vertebra and long bones (Figure 2, F and G). This low bone mass was associated with a >2-fold decrease in Ob.N/T.Ar. compared with WT mice, without any changes in osteoclast parameters (Figure 2F). These results demonstrated that B_{12} deficiency during aging in the offspring affects bone mass independent of body growth.

B_{12} deficiency causes GH resistance. Given that loss of B_{12} caused low bone mass and decreased osteoblast numbers in vivo, we considered the possibility that B_{12} may regulate osteoblast numbers and function by directly acting on these cells to regulate bone mass. To test this contention, we cultured primary osteoblasts in B_{12}-deficient medium, treated them with different doses of B_{12}, and measured their proliferation and differentiation. Reducing the concentration of B_{12} from 10,000 to 0 nM did not have any significant effect on proliferation or differentiation of osteoblasts (Supplemental Figure 3A). Consistent with these results, primary osteoblasts from B_{12}-deficient mice proliferated and differentiated equally well as WT cells (Supplemental Figure 3A). These in vitro results were surprising, in contrast to the in vivo results of a ≥3-fold decrease in osteoblast numbers and function in B_{12}-deficient animals, which suggests that B_{12} deficiency likely affects osteoblasts through an endocrine mechanism.

GH, a hormone made in the pituitary gland, appeared to be the likely candidate, given its role in postweaning growth and bone mass accrual (23, 27, 30). We therefore first analyzed serum levels of GH in 8-week-old WT and $Gif^{-/-}{}_{(F2)}$ mice. Serum GH levels were increased approximately 3-fold in mutants compared with WT mice (Figure 3A). This increase in GH in $Gif^{-/-}{}_{(F2)}$ animals was associated with increased expression of GH releasing hormone (*Ghrh*), which regulates pituitary GH production, in the hypothalamus (Figure 3B). These results suggested that B_{12}-deficient animals display GH resistance or insensitivity, at the level of either GH receptor (*Ghr*) or one of its downstream effectors, in the liver. Analysis of *Ghr* showed normal expression in the liver and bone in $Gif^{-/-}{}_{(F2)}$ animals; however, levels of serum IGF1 (through which GH mediates many of its peripheral actions) were reduced >4-fold (Figure 3, C and D). The decrease in IGF1 serum levels was associated with a decrease in IGF1 receptor (IGF1R) phosphorylation in the target tissues (Figure 3E).

Since *Igf1* expression is regulated by STAT5 signaling downstream of GH, we next investigated whether activation of STAT5 and its major targets is perturbed in $Gif^{-/-}{}_{(F2)}$ mice. In $Gif^{-/-}{}_{(F2)}$ mice, STAT5 phosphorylation was nearly absent in the liver and muscle, 2 major GH target tissues, but not in other tissues (Figure 3F). The decrease in STAT5 phosphorylation was associated with a major increase in expression of *Socs2*, an inhibitor of STAT5, in $Gif^{-/-}{}_{(F2)}$ liver (Figure 3G). In addition, mRNA levels of major STAT5 targets in the liver (31), such as IGF binding protein 1 (*Igfbp1*), was increased, whereas expression of *Igf1*, IGF binding protein acid labile subunit (*Igfals*), solute carrier organic anion transporter family member 1a1 (*Slco1a1*), major urinary proteins (*Mup1–Mup3*), and hydroxysteroid dehydrogenase 3b5 (*Hsd3b5*) was decreased

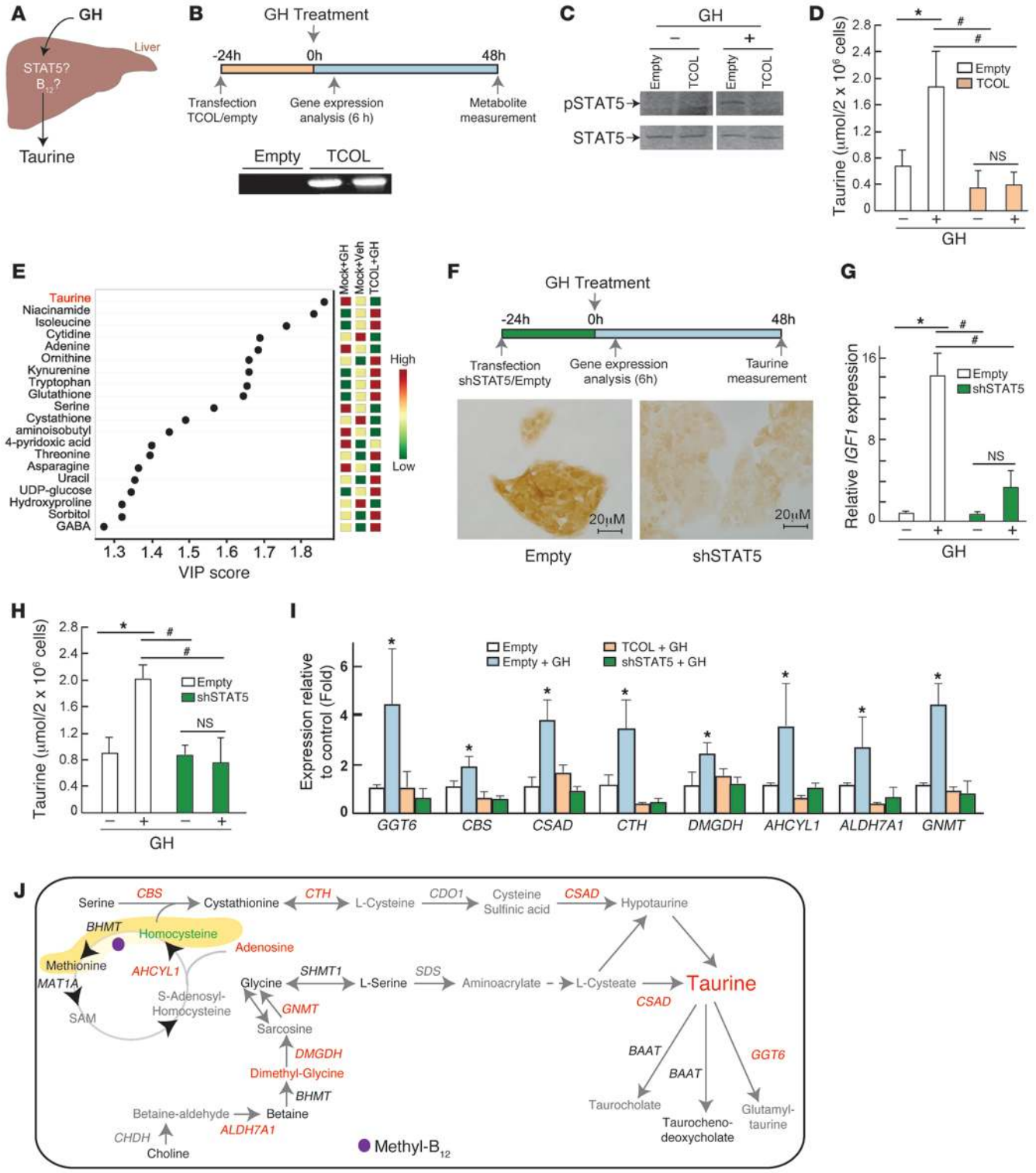
A
GH
Liver
STAT5?
B12?
Taurine
B
GH Treatment
-24h
0h
48h
Transfection TCOL/empty
Gene expression analysis (6 h)
Metabolite measurement
Empty
TCOL
C
GH
pSTAT5
STAT5
D
Taurine (μmol/2 x 10^6 cells)
Empty
TCOL
NS
E
Mock+GH
Mock+Veh
TCOL+GH
High
Low
Taurine
Niacinamide
Isoleucine
Cytidine
Adenine
Ornithine
Kynurenine
Tryptophan
Glutathione
Serine
Cystathione
aminoisobutyl
4-pyridoxic acid
Threonine
Asparagine
Uracil
UDP-glucose
Hydroxyproline
Sorbitol
GABA
VIP score
F
GH Treatment
Transfection shSTAT5/Empty
Gene expression analysis (6h)
Taurine measurement
20μM
Empty
shSTAT5
G
Relative IGF1 expression
Empty
shSTAT5
NS
H
Taurine (μmol/2 x 10^6 cells)
Empty
shSTAT5
NS
I
Expression relative to control (Fold)
Empty
Empty + GH
TCOL + GH
shSTAT5 + GH
GGT6
CBS
CSAD
CTH
DMGDH
AHCYL1
ALDH7A1
GNMT
J
Serine
CBS
Cystathionine
CTH
L-Cysteine
CDO1
Cysteine Sulfinic acid
CSAD
Hypotaurine
BHMT
Homocysteine
Adenosine
Methionine
AHCYL1
MAT1A
SAM
S-Adenosyl-Homocysteine
Glycine
SHMT1
L-Serine
SDS
Aminoacrylate
L-Cysteate
Taurine
CSAD
GNMT
Sarcosine
DMGDH
Dimethyl-Glycine
BHMT
Betaine-aldehyde
Betaine
ALDH7A1
CHDH
Choline
Methyl-B12
BAAT
GGT6
BAAT
Taurocholate
Taurocheno-deoxycholate
Glutamyl-taurine

Figure 5
GH regulates taurine synthesis in a STAT5- and B_{12}-dependent manner. (**A**) Relationship among taurine, STAT5, and B_{12} in the liver. (**B**) Experimental regimen used to test B_{12} involvement in GH regulation of taurine synthesis. Also shown is RT-PCR analysis to detect *Oleosin* transcript in the cells after transfection with empty vector or TCOL construct. (**C**) STAT5 phosphorylation upon GH treatment in empty vector– or TCOL-transfected HepG2 cells. Blots were run noncontiguously. (**D**) Taurine levels upon GH treatment in empty vector– or TCOL-transfected HepG2 cells. (**E**) PLSDA-VIP scores plot of metabolomics data from hepatocytes after empty or TCOL transfection. (**F**) Experimental regimen used to test STAT5 involvement in GH regulation of taurine production. Photomicrographs show immunohistochemistry of STAT5 in HepG2 cells transfected with nontargeting (empty) or STAT5 (shSTAT5) shRNA. (**G**) Relative expression of *IGF1* upon GH treatment in empty or STAT5 shRNA–transfected HepG2 cells. (**H**) Taurine levels upon GH treatment in empty or STAT5 shRNA–transfected HepG2 cells. (**I**) Real-time PCR analysis of enzymes in the taurine synthesis pathway in empty, TCOL, or STAT5 shRNA–transfected cells treated with vehicle or GH. (**J**) GH regulation of the taurine synthesis pathway. Red metabolites and genes, upregulated (only those upregulated by GH and that do not respond to GH upon STAT5 shRNA or TCOL transfection); green metabolites and genes, downregulated; black metabolites and genes, not altered; gray metabolites and genes, not measured. $^{*}P < 0.05$; $^{\#}P < 0.01$. Values are mean ± SEM. Scale bars: 20 μm (**F**). See also Supplemental Figure 5.

(Figure 3H and Supplemental Figure 3B), similar to previous observations in *Stat5*$^{-/-}$ mice (32). This GH resistance was also present in aged *Gif*$^{-/-}$$_{(F1)}$ mice, and maternal B_{12} injections normalized GH/IGF1 levels in *Gif*$^{-/-}$$_{(F2)}$ offspring (Supplemental Figure 3, C and D). These results revealed that B_{12} deficiency results in major abrogation of GH action in the offspring.

We next investigated how B_{12} deficiency abrogates GH action, using liver tissue as a model. B_{12} derivatives in mammals act as cofactors for the function of only 2 known enzymes, MTR and MUT (Figure 3I); therefore, we first measured the metabolites downstream of these enzymes to observe the effect of B_{12} deficiency on their function. Methionine, a product of MTR, was significantly downregulated, and its substrate, homocysteine, was increased, whereas succinate, a downstream product of MUT, was not affected (Figure 3J). Methionine is a precursor for cellular production of S-adenosyl methionine (SAM), which is an essential methyl donor for histone and DNA methylation, 2 epigenetic modifications known to affect basal and ligand-stimulated gene expression levels (33). Because we observed a major decrease in the expression of liver *Igf1*, we first tested whether B_{12} deficiency alters the methylation status of this gene, using histone methylation as a marker. ChIP analysis of histone methylation in WT and *Gif*$^{-/-}$$_{(F2)}$ liver tissues revealed a major decrease in histone (H3) methylation at the *Igf1* locus (Figure 3K). These results suggested that a major decrease in histone methylation might lead to decreased responsiveness of target tissues to GH, resulting in development of GH resistance.

If the observed decrease in liver IGF1 synthesis alone is necessary and sufficient to cause growth retardation and osteoporosis in *Gif*$^{-/-}$$_{(F2)}$ animals, then IGF1 administration to these animals should be able to overcome their growth retardation. To examine this possibility, we treated *Gif*$^{-/-}$$_{(F2)}$ animals beginning at P20 with twice-daily injections of recombinant IGF1, which has previously been shown to prevent and/or cure growth abnormalities (34). To our surprise, IGF1 treatment led to early lethality of *Gif*$^{-/-}$$_{(F2)}$ animals (Figure 3L). This extreme response to IGF1 can be explained by the lower basal glucose levels observed in these animals (15.1 ± 1.2 versus 25.5 ± 3.2 nM), likely due to GH resistance, and IGF1 administration further decreased their glycemic state (5.2 ± 1.3 nM; at this point, if animals were given a bolus of glucose, reviving them and preventing death), likely resulting in lethality (Figure 3L). Moreover, administration of SAM that normalized DNA methylation could not rescue the growth retardation and bone abnormalities caused by B_{12} deficiency (data not shown). These results suggest that the suppression and/or activation of another GH mediator in addition to SAM (dependent on B_{12}, either acting independently or regulating IGF1 action) underlies GH resistance in B_{12}-deficient animals.

Identification of taurine as a critical metabolite positively regulated by B_{12}. To identify the mediators underlying the GH resistance observed upon B_{12} deficiency, we next carried out targeted metabolomic analysis in the liver of *Gif*$^{-/-}$$_{(F2)}$ mice and compared this profile with GH-regulated metabolome. Analysis of metabolomic data upon B_{12} deficiency revealed that most of the metabolites were downregulated and were involved in amino acid, betaine, primary bile acid, protein, and purine metabolism (Figure 4A and Supplemental Figure 4A). Metabolite profiling of GH-treated hepatocytes identified many metabolites that showed similar positive regulation by GH and B_{12} (Figure 4A and Supplemental Figure 4B) and might underlie the GH resistance observed upon B_{12} deficiency.

Quantitative enrichment analysis on B_{12}-deficient metabolome showed major perturbations in the metabolic pathways associated with taurine and hypotaurine, folate and bile acid biosynthesis, nucleotide and amino acid metabolisms, and protein synthesis (Figure 4B). Pathway analysis identified that the taurine and hypotaurine pathways had a substantial effect on cellular function following B_{12} deficiency (Figure 4C). To identify which metabolites contribute to the group separation of WT and B_{12}-deficient samples, we performed a supervised multivariate regression technique, partial least squares discriminant analysis (PLSDA). In the PLSDA model, the number of latent variables (LVs) to be used depends on the sum of squares captured by the model (R^2), cross-validated R^2 (Q^2), and prediction accuracies based on cross-validations, with different numbers of LVs. Variable importance in projection (VIP) is one of the important measures of PLSDA, where it is a weighted sum of squares of the PLS loadings taking into account the amount of explained class variation in each dimension. PLSDA-VIP analysis of the liver metabolomics data identified that taurine had the highest VIP score and could serve as a biomarker for B_{12}-deficient status (Figure 4D). Consistent with the notion that perturbation in taurine metabolism underlies the GH resistance observed upon B_{12} deficiency, measurement of taurine and its derivatives in *Gif*$^{-/-}$$_{(F2)}$/$B_{12}$ liver showed complete rescue of these metabolites to the levels seen in WT liver (Figure 4E). Moreover, further suggesting a critical role of taurine in the GH/B_{12}-dependent pathway, taurine deficiency has previously been shown to be associated with GH/IGF1 signaling downregulation in Ames dwarf mice (35), and methionine metabolism is significantly perturbed in patients with GH deficiency (36).

Taken together, these integrated metabolomic analysis in WT and *Gif*$^{-/-}$$_{(F2)}$ mouse liver identified a hitherto-unanticipated suppression of taurine metabolism in B_{12} deficiency–mediated GH resistance.

GH regulates taurine synthesis in a STAT5/B_{12}-dependent manner. Thus far, our results provided correlative evidence that B_{12} deficiency in the liver results in reduced taurine production associated with abrogation of GH signaling. We next generated in vitro

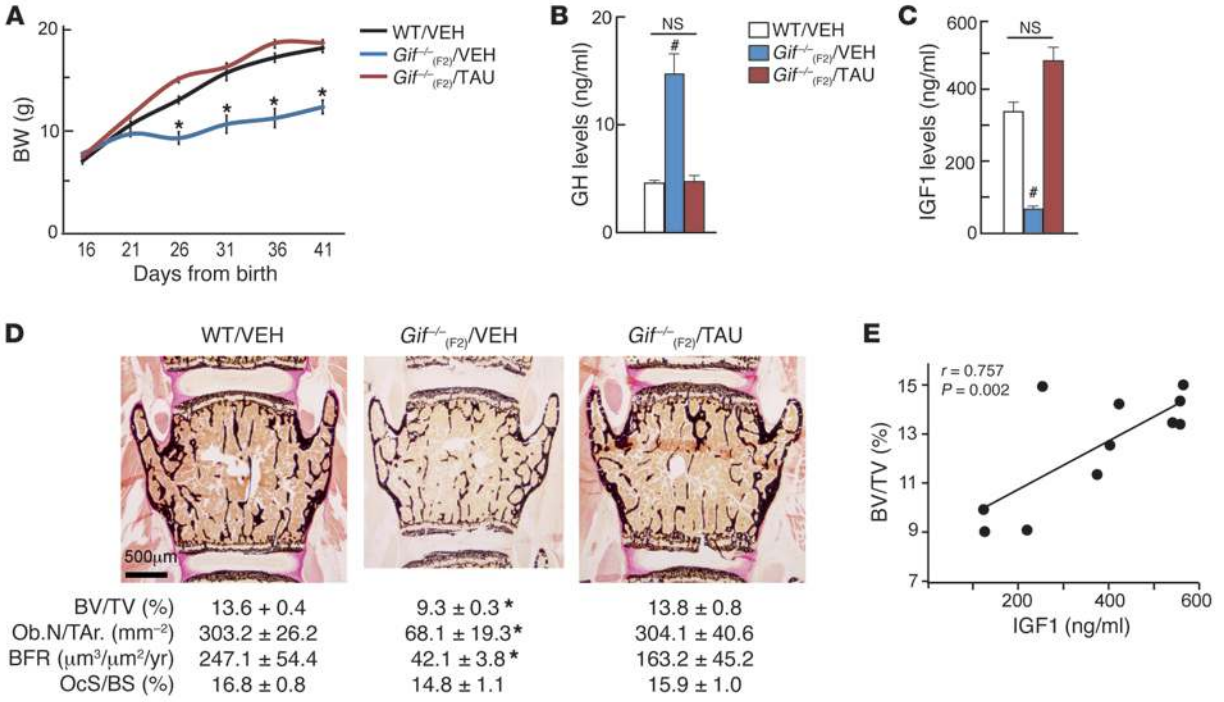

Figure 6

Oral taurine administration prevents growth retardation and osteoporosis in *Gif*$^{-/-}_{(F2)}$ mice. (**A**) Growth curve analysis of WT/VEH, *Gif*$^{-/-}_{(F2)}$/VEH, and *Gif*$^{-/-}_{(F2)}$/TAU mice. (**B** and **C**) Serum GH (**B**) and IGF1 (**C**) levels in WT/VEH, *Gif*$^{-/-}_{(F2)}$/VEH, and *Gif*$^{-/-}_{(F2)}$/TAU mice. (**D**) Histological analysis of vertebra in WT, *Gif*$^{-/-}_{(F2)}$/VEH, and *Gif*$^{-/-}_{(F2)}$/TAU mice, with quantification of BV/TV, Ob.N/T.Ar., BFR, and OcS/BS. (**E**) Pearson correlation scatter plot between BV/TV and serum IGF1 levels in taurine-treated mice. $^{*}P < 0.05$; $^{\#}P < 0.01$. $n = 5$ per group. Values are mean ± SEM. Scale bar: 500 μm. See also Supplemental Figure 6.

models of B_{12} and STAT5 deficiency in hepatocytes and asked whether GH/STAT5 signaling regulates taurine production and, if so, whether this process is affected by B_{12} deficiency (Figure 5A). We used 2 strategies to investigate this question. First, to investigate the B_{12} regulation of GH-dependent taurine synthesis, we used a sequestration approach to ablate B_{12} action in hepatocytes using overexpression of a transcobalamin 2–oleosin construct (TCOL) in HepG2 cells. Upon expression, TCN2 binds to B_{12} in the cytoplasm, and oleosin immobilizes this TCN2-B_{12} complex to the endoplasmic reticulum, thereby chelating any B_{12} present in the cytosol (37). To this end, we synthesized TCOL fusion vectors and created stably transfected HepG2 cells with TCOL or an empty vector as a control. Measurement of *Oleosin* transcript in the cells showed that we successfully overexpressed TCOL (Figure 5B). Measurement of taurine in the transfected cells showed that while GH treatment significantly increased pSTAT5 and taurine production in the vector-transfected cells, this increase in pSTAT5 and taurine was completely abrogated in TCOL-transfected cells (Figure 5, C and D). PLSDA-VIP analysis of the metabolomics data derived from these cells showed that, once again, taurine was the main driver for the separation of the 3 groups (Figure 5E). Importantly, addition of taurine to TCOL-transfected cells fully restored GH responsiveness, as measured by IGF1 expression analysis (Supplemental Figure 5A).

The observations that B_{12}-deficient animals had a major decrease in STAT5 phosphorylation, and that GH increased taurine production, led us to next investigate whether GH — through STAT5 signaling — regulates taurine production. We stably transfected hepatocytes (HepG2 cells) with shRNA against STAT5 or empty vector, followed by treatment of these cells with either vehicle or GH. Immunohistochemical analysis of STAT5 levels in these cells after transfection revealed that STAT5 expression was successfully abrogated in STAT5 shRNA–transfected compared with mock-transfected cells (Figure 5F). Measurement of *IGF1* expression confirmed that we successfully abrogated GH action (Figure 5G). We next measured taurine production in response to GH. GH treatment significantly increased taurine production in the mock-transfected cells, but this increase was completely abrogated in STAT5 shRNA–transfected cells (Figure 5H).

Finally, we questioned which of the enzymes in the taurine synthesis pathway are regulated by GH in a STAT5- and B_{12}-dependent manner. GH treatment of hepatocytes lead to an increase in the expression of gamma-glutamyltransferase 6 (*GGT6*), cystathionine beta synthase (*CBS*), cysteine sulfinic acid decarboxylase (*CSAD*), dimethylglycine dehydrogenase (*DMGDH*), S-adenosylhomocysteine hydrolase-like 1 (*AHCYL1*), aldehyde dehydrogenase 7 family, member A1 (*ALDH7A1*), and glycine N-methyltransferase (*GNMT*), while it did not affect expression of other enzymes (*BHMT*, *SHMT1*, *BAAT*, and *MAT1A*) in this pathway (Figure 5I and data not shown). The increase in expression of these enzymes observed upon GH treatment was abrogated following loss of STAT5 (STAT5 shRNA) or with sequestration of B_{12} in the cells (Figure 5I). Integrated analysis of GH-regulated metabolites and gene expression changes linking methionine to taurine metabolism showed that GH signaling affected taurine biosynthesis pathway at multiple levels (Figure 5J).

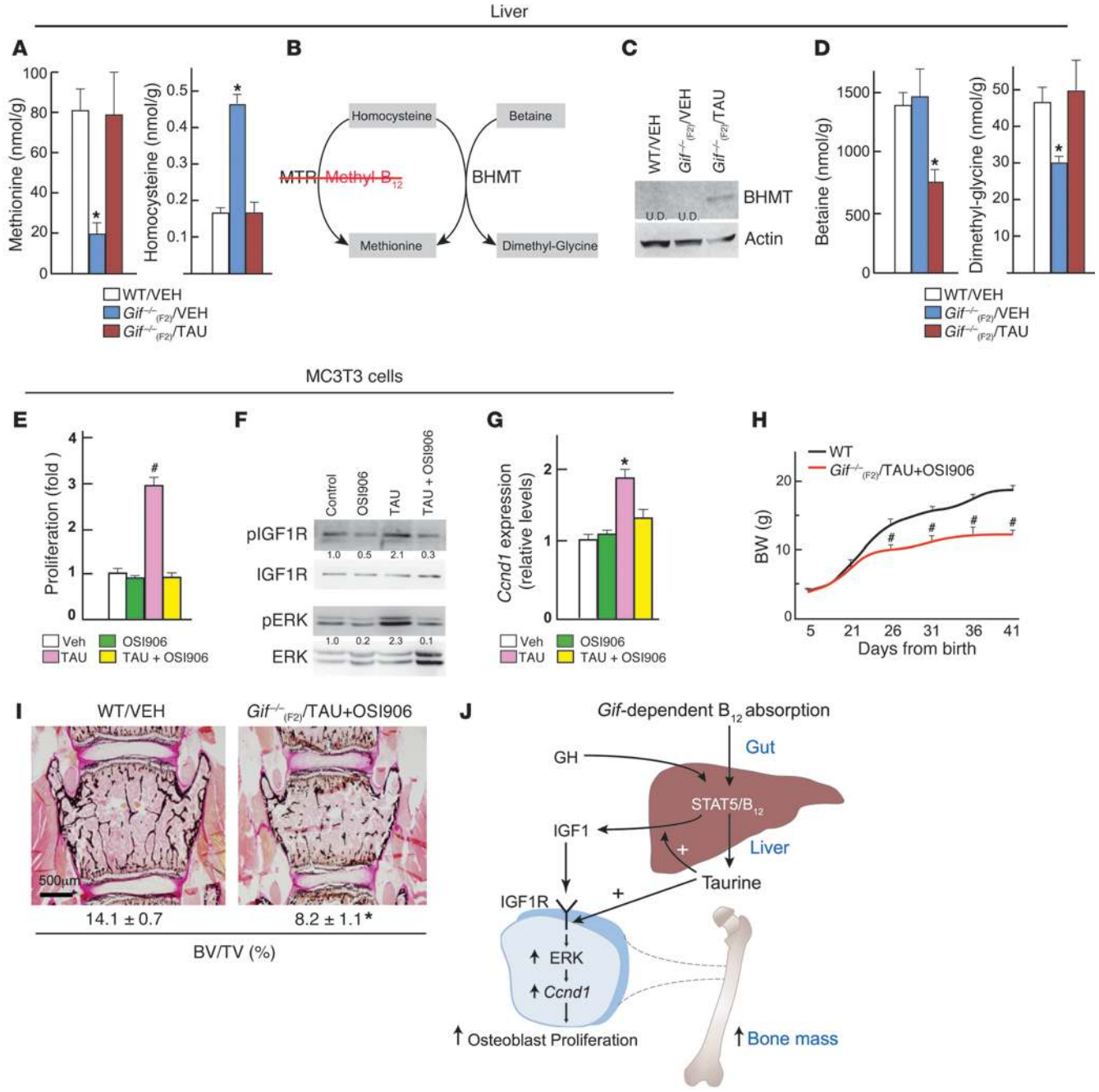

Figure 7

Taurine increases IGF1 synthesis from liver and its action in osteoblasts to regulate bone mass. (**A**–**D**) Liver samples. (**A**) Levels of methionine and homocysteine in WT, *Gif*$^{-/-}_{(F2)}$/VEH, and *Gif*$^{-/-}_{(F2)}$/TAU liver. (**B**) B_{12}-dependent (MTR) and -independent (BHMT) methionine synthesis pathways. (**C**) Western blot analysis of BHMT levels in WT, *Gif*$^{-/-}_{(F2)}$/VEH, and *Gif*$^{-/-}_{(F2)}$/TAU liver. Lanes were run contiguously. U.D., undetectable. (**D**) Levels of betaine and dimethyl-glycine in liver of WT, *Gif*$^{-/-}_{(F2)}$/VEH, and *Gif*$^{-/-}_{(F2)}$/TAU mice. (**E**–**G**) MC3T3-E1 osteoblast cells. Changes in BrdU incorporation (**E**), IGF1R and ERK phosphorylation (**F**), and *Ccnd1* expression (**G**) in cells treated for 24 hours with vehicle, OSI906, taurine, or taurine plus OSI906. Lanes in **F** were run contiguously, and blots were stripped and reprobed with IGF1R or ERK. Relative quantification of pIGF1R and pERK (normalized to IGF1R and ERK, respectively) is shown below. A representative blot from 3 different experiments is shown. (**H**) Growth curve analysis of WT and *Gif*$^{-/-}_{(F2)}$/TAU+OSI906 mice (n = 5 each). (**I**) Bone mass analysis (BV/TV) in the vertebra of WT and *Gif*$^{-/-}_{(F2)}$/TAU+OSI906 mice (n = 5 per group). (**J**) Gut/liver/bone endocrine axis, illustrating GH/STAT5/B_{12}-dependent changes in serum IGF1 and taurine that regulate osteoblast proliferation and bone mass. *P < 0.05; #P < 0.01. Values are mean ± SEM. Scale bar: 500 μm. See also Supplemental Figure 7.

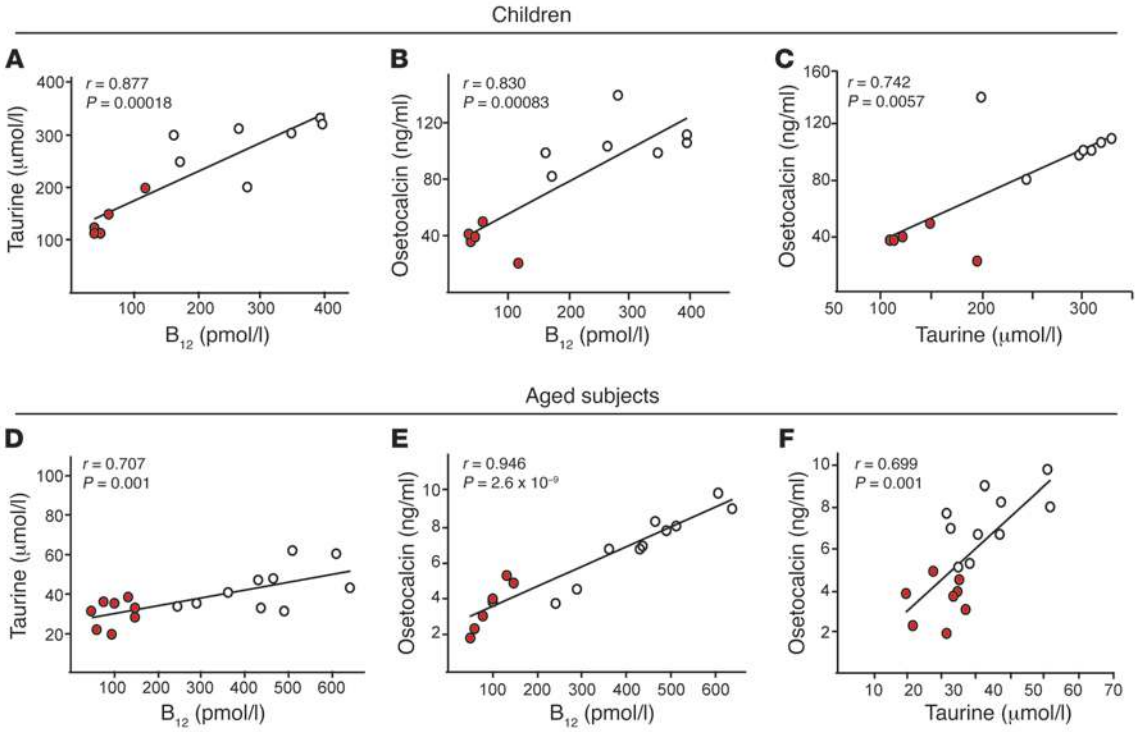

Figure 8

B_{12} status correlates with taurine and the bone formation marker osteocalcin during early postnatal life and aging in humans. (**A**–**F**) Pearson correlation scatter plots between (**A** and **D**) serum B_{12} and taurine, (**B** and **E**) B_{12} and osteocalcin, and (**C** and **F**) osteocalcin and taurine in (**A**–**C**) children of B_{12}-deficient mothers (red symbols; $n = 5$) and of healthy mothers (white symbols; $n = 7$) and in (**D**–**F**) aged B_{12}-deficient subjects (red symbols; $n = 8$) and healthy controls (white symbols; $n = 10$). Pearson R as well as P values are shown. See also Supplemental Figure 8.

Based on these results, we concluded (a) that GH increases taurine production in the hepatocytes in a STAT5- and B_{12}-dependent manner and (b) that STAT5 and B_{12} regulate taurine synthesis by regulating expression of critical enzymes and metabolites in the taurine synthesis pathway. Together, these results showed that GH signals in the hepatocytes in a STAT5/B_{12}-dependent manner to regulate production of taurine, whose deficiency in B_{12}-deficient animals might underlie GH resistance and osteoporosis.

Oral feeding of taurine to B_{12}-deficient Gif$^{-/-}$(F2) offspring normalizes the GH/IGF1 axis and prevents their growth retardation and osteoporosis. If the decrease in taurine levels is the cause of GH resistance and low bone mass phenotype in Gif$^{-/-}$(F2) animals, then administration of taurine to these animals should be able to prevent postweaning growth and bone mass abnormalities. To this end, 16-day-old WT and Gif$^{-/-}$(F2) females were given either vehicle or 500 mg/kg BW taurine daily (orally) [referred to herein as Gif$^{-/-}$(F2)/VEH and Gif$^{-/-}$(F2)/TAU mice, respectively]. Growth curve analysis showed that although Gif$^{-/-}$(F2)/VEH offspring showed growth retardation from P21 to P26, Gif$^{-/-}$(F2)/TAU mice grew normally between P21 and P26 and thereafter, and were in fact indistinguishable from WT animals (Figure 6A). This rescue of growth retardation in Gif$^{-/-}$(F2)/TAU animals was associated with normalization of serum GH and IGF1 levels, which were restored to the levels seen in WT animals (Figure 6, B and C). PLSDA analysis of liver metabolite profiles revealed that Gif$^{-/-}$(F2)/TAU mice clustered with the WT mice, whereas Gif$^{-/-}$(F2)/VEH mice were clearly distinct from these 2 groups (Supplemental Figure 6A). This rescue of liver metabolome was also reflected in 2-way clustering performed on the metabolite profiles (Supplemental Figure 6B). Histological and histomorphometry analysis of bone from 8-week-old WT, Gif$^{-/-}$(F2)/VEH, and Gif$^{-/-}$(F2)/TAU mice revealed that the low bone mass observed in Gif$^{-/-}$(F2)/VEH mice was completely rescued in Gif$^{-/-}$(F2)/TAU mice, due to a major increase in osteoblast number and function, while osteoclast parameters were not affected (Figure 6D and Supplemental Figure 6C). Thus, daily oral administration of taurine to B_{12}-deficient offspring prevented the growth retardation and low bone mass caused by B_{12} deficiency. These results indicated that taurine is an essential downstream mediator of B_{12}-dependent GH signaling in the regulation of growth and bone metabolism. The observation that rescue of growth and bone mass abnormalities in taurine-treated B_{12}-deficient mice was associated with a major increase in serum levels of IGF1, a major regulator of osteoblast function, led us to next investigate the importance of IGF1 signaling in this process. We performed a correlation analysis between bone mass or osteoblast numbers and serum levels of IGF1 to investigate whether IGF1 signaling contributes to the changes in bone mass in taurine-fed B_{12}-deficient animals. This analysis showed a linear correlation between serum IGF1 levels and bone mass or osteoblast numbers in taurine-fed animals (Figure 6E and Supplemental Figure 6D). Together, these results suggest that IGF1 synthesis from the liver and its action in IGF1 target tissues underlies taurine-mediated rescue of growth retardation and osteoporosis in Gif$^{-/-}$(F2) mice.

Taurine increases IGF1 synthesis in hepatocytes and its action in osteoblasts to regulate bone mass. We next investigated the mechanisms through which taurine affects liver IGF1 synthesis downstream

of GH to regulate bone mass. The taurine-mediated increase in IGF1 synthesis suggested that taurine was able to overcome the consequences of B_{12} deficiency in the liver. Analysis of metabolite levels in the liver showed that methionine levels in taurine-treated animals were rescued to the levels seen in WT animals (Figure 7A). Because MTR, the principle enzyme that synthesizes methionine in mammals, cannot function in the absence of B_{12}, we looked at alternate pathways of methionine synthesis that are not dependent on B_{12} as a cofactor and could explain the increase in methionine synthesis in response to taurine. Analysis of protein levels and activity of betaine-homocysteine S-methyltransferase (BHMT), an enzyme that carries out a parallel reaction to synthesize methionine, revealed a major increase in its protein levels in the liver of taurine-fed animals (Figure 7, B and C). Consistent with the increased protein levels of BHMT, its substrates (betaine and homocysteine) were decreased, whereas its products (dimethylglycine and methionine) were increased, in liver (Figure 7, B and D). *Bhmt* expression was found to be undetectable in bone (Supplemental Figure 7A). ChIP analysis of me2K36, a marker of histone methylation levels, at the *Igf1* locus showed that this increase in methionine levels normalized the methylation status of *Igf1* in the liver (Supplemental Figure 7B). In contrast to the changes in liver *Igf1*, methylation status of *Igf1* in osteoblasts or its expression in the long bone was not different among WT, $Gif^{-/-}{}_{(F2)}$/VEH, and $Gif^{-/-}{}_{(F2)}$/TAU mice (Supplemental Figure 7, C and D). Together, these results revealed that taurine-mediated BHMT pathway activation led to the restoration of methylation status and responsiveness of *Igf1*, and other genes, to circulating GH.

Next, we investigated which aspects of osteoblast biology are affected by taurine, and whether taurine's effect is dependent on IGF1 signaling. Taurine treatment (20 mM) specifically increased osteoblast proliferation, but had no effect on the differentiation or mineralization of these cells, and this increase in osteoblast proliferation was blocked by pretreatment with the IGF1R antagonist OSI906 (10 μM) (Figure 7E and Supplemental Figure 7, E–G). Analysis of signaling pathways downstream of taurine in osteoblasts revealed an increase in IGF1R phosphorylation and downstream activation of the ERK pathway, as reflected by increased pERK levels and increased expression of its transcriptional target, *Ccnd1*, both of which were abrogated by OSI906 pretreatment (Figure 7, F and G). This effect of taurine on IGF1R signaling was also seen in the long bone in vivo (Supplemental Figure 7, H and I). These results showed that taurine stimulates the IGF1R/ERK signaling cascade to increase osteoblast proliferation.

Finally, to investigate the importance of IGF1R in mediating the bone and growth abnormalities in $Gif^{-/-}{}_{(F2)}$ mice, we treated these mice with either vehicle [$Gif^{-/-}{}_{(F2)}$/VEH] or taurine plus OSI906 (50 mg/kg BW/d) [$Gif^{-/-}{}_{(F2)}$/TAU+OSI906] from P16 onward. Growth curve and bone histomorphometric analyses showed that $Gif^{-/-}{}_{(F2)}$/TAU+OSI906 mice remained growth retarded and osteoporotic (Figure 7, H and I). These results indicated that B_{12}/taurine is an essential mediator of GH action that increases IGF1 synthesis from the liver and its signaling in osteoblasts to increase osteoblast proliferation and bone mass while it increases GH signaling in other tissues, such as cartilage, which is dependent on GH directly to increase longitudinal growth (Supplemental Figure 7J).

Evidence for the B_{12}/taurine/bone pathway in children and aged patients with B_{12} deficiency. Serum samples from children born of nutritionally B_{12}-deficient mothers showed a significant decrease in their serum B_{12}, taurine, and osteocalcin (as a marker of bone formation) levels compared with age-matched controls (Supplemental Figure 8, A and B). Correlation analysis using all samples showed a significant positive correlation between variation in serum B_{12} and taurine ($R = 0.877$, $P = 0.00018$), B_{12} and osteocalcin ($R = 0.830$, $P = 0.00083$), and taurine and osteocalcin ($R = 0.742$, $P = 0.0057$) levels (Figure 8, A–C).

Analysis of aged patients with B_{12} deficiency showed significantly decreased levels of taurine and osteocalcin (Supplemental Figure 8C). Further correlation analysis using all samples from aged subjects showed significant positive correlation between variation in serum B_{12} and taurine ($R = 0.707$; $P = 0.001$), B_{12} and osteocalcin ($R = 0.946$, $P = 2.6 \times 10^{-9}$), and taurine and osteocalcin ($R = 0.699$; $P = 0.0012$) levels (Figure 8, D–F). These data provide further support for a physiological role of B_{12} in regulating taurine synthesis and bone formation in humans. However, the human sample size in our studies was small; follow-up controlled clinical trials correlating the markers of the B_{12}/taurine axis with bone formation using larger sample sizes would be needed.

Discussion

Our present findings uncovered an unanticipated regulation of growth and bone mass through a vitamin. These findings shift the focus to maternal nutritional milieu as a major player in skeletogenesis and provide conclusive evidence that maternally derived B_{12} regulates growth and bone accrual in the offspring via the GH/IGF1 axis.

Our studies demonstrating an effect of B_{12} derived from the mother on postnatal skeletogenesis of the offspring increases the repertoire of maternal effects on organ growth and bone mass. To our knowledge, B_{12} is the first vitamin of maternal origin whose deficiency or excess specifically manifests its consequence on postweaning bone formation. Our conclusion that alterations in maternal ability to transfer B_{12} to the offspring regulated growth and bone mass acquisition was based on 2 lines of evidence. First, only pups born from homozygous $Gif^{-/-}$ mothers, not those born from heterozygous $Gif^{+/-}$ mothers, had early-onset growth retardation and osteoporosis. Second, a single injection of B_{12} to the homozygous mothers was able to transfer sufficient B_{12} to their progeny and prevented the development of growth retardation and osteoporosis. The onset of growth retardation in the offspring only after weaning indicated that only minimal B_{12} is required during critical periods of pregnancy for functional folate/methionine metabolism. A recent study reported that mutated methionine synthase reductase (*Mtrr*), which activates the MTR/B_{12} complex, caused transgenerational embryonic abnormalities and/or lethality that were much more severe than our B_{12}-deficient mouse model (38). On the other hand, in our present study, the higher stability of B_{12} overcame this neonatal lethality and allowed us to investigate the effects of deficiency in methionine/folate metabolism on mouse postnatal growth and metabolism. Together, our results indicate that modifications in methionine/folate metabolism during development or postnatal life will have long-lasting consequences on growth and bone homeostasis.

B_{12} deficiency results in ablation in the activity of the enzymes MTR and MUT in mammals and, consequently, accumulation of their substrates, including homocysteine and methylmalonic acid (MMA), respectively. The observation that increased homocysteine and MMA levels in serum and tissues upon B_{12} deficiency have diverse effects on multiple intracellular pathways led us to investigate whether the B_{12} deficiency–mediated growth retardation and low bone mass observed during P21–P46 was caused by their

accumulation. Administration of homocysteine (50 mg/kg/d i.p.) or MMA (1 μmol/g BW/d i.p.) to WT mice beginning at P21 for 4 weeks, the period during which we observed growth retardation upon B_{12} deficiency, had no effect on the growth or bone mass of WT animals (Supplemental Figure 3, E and F). These results were consistent with prior reports that postnatal administration of MMA does not affect growth of rats (39). Our findings suggest that the growth retardation and low bone mass in B_{12}-deficient animals observed from P21 was not caused by accumulation of MMA or homocysteine, but rather by downregulated production of other B_{12}-dependent downstream metabolites. However, it is possible that the dose and duration of treatments used herein did not saturate the intracellular compartments of MMA or homocysteine, and that further increasing their levels, or levels of other metabolites, for longer durations may affect cellular processes underlying growth. Finally, our finding that taurine administration rescued the molecular and cellular abnormalities observed upon B_{12} deficiency suggested that taurine synthesis lies upstream of the metabolites perturbed upon B_{12} deficiency.

Analysis of *Gif* mutants for 2 generations showed that maternally derived B_{12} profoundly regulated GH-dependent processes in the offspring. Investigation into the GH resistance of B_{12}-deficient mutants lead to the identification of major liver metabolic pathways underlying this resistance. Multiple lines of evidence provide credence to our assertion that the decrease in bone mass and organ growth observed upon B_{12} deficiency is caused, at least in part, by GH resistance. First, B_{12}-deficient mice closely phenocopy $Ghr^{-/-}$ and $Stat5^{-/-}$ mice (32, 40). These mutant mice have similar changes in hepatic gene expression, including reduced *Igf1*, *Igfals*, *Mup1*, *Slco1a1*, and *Hsd3b5* mRNA and increased *Igfbp1*. Second, both B_{12}-deficient and $Stat5^{-/-}$ mice show a major decrease in serum IGF1 levels. Third, there was a 10% reduction in serum total protein content in B_{12}-deficient mice (40.1 ± 5.1 g/l, versus 50.4 ± 4.0 g/l in WT), an observation consistent with a major reduction in GH-mediated anabolic processes such as protein synthesis. Taken together, the striking similarities between B_{12}-deficient and $Stat5^{-/-}$ mice strongly support the notion that the effects of B_{12} deficiency, at least on growth and bone mass, are mediated by abrogation of STAT5-dependent signaling downstream of GH.

Investigation into the downstream mediators of GH action that underlie growth retardation and osteoporosis in B_{12}-deficient animals led to the discovery of taurine as a metabolite regulated by B_{12} and underlying GH resistance in B_{12}-deficient offspring. Taurine is a poorly understood amino acid whose function in body physiology has not been clear. Our demonstration that one means by which GH regulates growth and bone mass is through regulation of B_{12}-dependent liver taurine production is supported by 3 lines of evidences. First, taurine production was regulated by GH in hepatocytes in a STAT5- and B_{12}-dependent manner, because in the absence of either, GH was unable to increase taurine production. Second, taurine increased IGF1 synthesis from the liver and its action on osteoblasts by regulating IGF1R signaling. Third, feeding taurine to B_{12}-deficient animals prevented their growth retardation and osteoporosis by normalizing their GH resistance through the activation of an alternate methionine synthesis pathway (BHMT). Our finding that B_{12} deficiency or taurine administration did not affect *Igf1* expression in bone, but did so profoundly in the liver (Supplemental Figure 7, B–D), suggests that liver is much more sensitive to changes in B_{12} levels than bone. This is further supported by our in vitro results wherein B_{12} deficiency in osteoblasts did not affect their proliferation or function, whereas it led to hepatocyte dysfunction. We note that B_{12} deficiency or taurine-mediated rescue of bone mass was not associated with changes in mRNA levels of markers of osteoblast differentiation. It is likely that taurine affects osteoblast differentiation markers more profoundly at the level of mRNA translation/protein synthesis, a major function regulated by the GH/IGF1 axis. This explanation is supported by our finding that protein levels of OCN, a marker of osteoblast differentiation, were affected by changes in B_{12}/taurine levels, whereas mRNA levels of *Ocn* were not (Supplemental Figure 7, F and G). Finally, our identification of taurine synthesis from the liver as an essential process, in the absence of which IGF1 could not rescue growth and bone mass downstream of B_{12}, revealed an unanticipated role of taurine as an upstream regulator of IGF1 synthesis and action, further expanding the importance of IGF1 in body physiology (27).

In summary, our present findings (a) show an unanticipated regulation of growth and bone mass by maternally derived B_{12} through regulation of the GH/IGF1/taurine axis in the offspring; (b) identify the cellular and metabolic abnormalities associated with B_{12} deficiency; (c) show that taurine synthesis in the liver lies upstream of IGF1 synthesis and action and is necessary and sufficient to prevent the growth retardation and osteoporosis observed upon B_{12} deficiency; and (d) demonstrate that taurine mediates its action on growth and bone mass through regulation of IGF1 synthesis from the liver and its action in bone. Together, these in vitro and in vivo results support the concept that B_{12} regulates growth and bone mass through the regulation of GH sensitivity in the offspring by regulating liver taurine production, and increase the importance of the role played by liver in regulating whole-body physiology (41).

Our identification of a novel gut/liver/bone endocrine axis (Figure 7J) as a regulator of growth and bone mass raises several questions. First, what are the molecular regulators of B_{12} absorption and the molecules that are coabsorbed with it in the body physiology? Second, are there other vitamins that affect bone formation through similar maternal mechanisms? Third, what are the other effects of B_{12} on body physiology? Fourth, how does taurine increase BHMT levels and activity, and are there other metabolites that can perform the same function? Finally, as suggested by the profound positive influence of B_{12} on bone formation, could regulation of B_{12} and/or its downstream effector taurine have the potential to increase bone formation to treat skeletal diseases? Addressing these questions will require further investigation into the regulatory mechanisms that surround B_{12} physiology and the GH/taurine axis, and may lead to the development of novel therapies to cure growth and bone diseases.

Methods

Animals

$Gif^{-/-}$ mice ($Gif^{tm1aWtsi/tm1aWtsi}$), generated by the Sanger Mouse Genetics Programme, carry a knockout-first allele in which a promoterless cassette including *LacZ* and *neo* was inserted in *Gif*, resulting in a loss-of-function allele. $Gif^{-/-}$ mice were generated as part of the mouse genetics project using C57BL/6N embryonic stem cells and were on a pure C57 background. WT littermate controls were used throughout the study.

For CN-B_{12} treatment to pregnant dams, virgin $Gif^{-/-}{}_{(F1)}$ females were timed mated with $Gif^{-/-}{}_{(F1)}$ male mice. Pregnant animals received either vehicle (saline) or 200 μg CN-B_{12} (s.c.) on 12.5 dpc. Where indicated, WT and $Gif^{-/-}{}_{(F1)}$ offspring were treated orally with taurine (500 mg/kg/d) and/

or the IGF1R antagonist OSI906 (50 mg/kg BW/d) from P16. Mice were culled at the indicated ages.

μCT and skeletal analyses

μCT analysis was performed using a Skyscan 1172 μCT system with standard software provided by the manufacturer (Skyscan). Histological analyses (Osteomeasure Analysis System; Osteometrics) and skeletal preparations were performed as described previously (42, 43). 6–12 animals were analyzed per group (see Supplemental Methods and figure legends).

Cell cultures and molecular assays

Primary osteoblasts or MC3T3 cells were cultured in B_{12}-deficient medium or/and α-MEM, and cell proliferation (BrdU Cell Proliferation ELISA; Roche Applied Science) and differentiation (SensoLyte pNPP Alkaline Phosphatase Assay kit; AnaSpec Inc.) was performed as described previously (43). Western blot analysis was performed using standard methods using antibodies from Cell Signaling.

Human hepatoma HepG2 cells grown in α-MEM were stably transfected with STAT5b (SureSulencing shRNA Plasmid Kit; Qiagen) or TCOL (ref:_00DA0IMFs._500A0Bty7J; Origene) or with empty vector (mock) using Attractene (ShRNA) or Turbofect (plasmids).

Metabolomics and serum B_{12} analysis

Polar metabolites were extracted from mouse liver and cell samples, separated using Waters Acquity ultra performance liquid chromatography and, analyzed using triple quadrupole mass spectrometry. Serum B_{12} levels were analyzed using competitive immunoassay on a Siemens ADVIA Centaur Immunoassay analyzer. See Supplemental Methods for details.

Quantitative RT-PCR analysis

Total RNA was extracted using a Qiagen RNA extraction kit, and real-time PCR was performed using standard protocols.

Bioassays

Serum was prepared using BD Vacutainer SST, snap-frozen in liquid nitrogen, and stored at –80°C until analyzed. Serum GH was measured using Mouse Growth Hormone ELISA (Millipore Inc.), and IGF1 was measured using IGF1 Mouse/Human ELISA Kit (Abcam Inc.). Luciferase reporter assays were carried out using standard methods.

Human subjects

Children. All clinical evaluations and sample collections were performed by an experienced hematologist. Infants 3–24 months of age presenting with megaloblastic anemia and/or symptoms of B_{12} deficiency (weakness, failure to thrive, refusal to wean, vomiting, developmental delay, irritability, and tremor) were enrolled during their admission to the outpatient clinics of pediatrics and pediatric hematology of Kocaeli University Hospital. Infants with serum B_{12} levels <150 pmol/l were eligible for the study. Dietary history in the infants, especially consumption of breast milk and animal proteins (milk, yogurt, eggs, chicken, fish, and other meat products), as well as intake of vitamin pills during pregnancy/lactation in the mothers, was recorded.

Aged subjects. All samples used in this study were from the Kuopio Ischaemic Heart Disease Risk Factor Study (KIHD study), an ongoing, population-based cohort study to investigate the risk factors for coronary heart diseases, atherosclerosis, and other related outcomes in the Eastern Finnish population (44), and were donated by J. Kauhanen and T. Nurmi (University of Eastern Finland, Kuopio, Finland). Subjects with B_{12} levels <150 pmol/l were considered the B_{12}-deficient group (45). According to this classification, 8 subjects in the B_{12}-deficient group and 10 controls (age and gender matched) were included in this study. Clinical characteristics of the subjects are given in Supplemental Figure 8.

Statistics

Results are given as mean ± SEM. Statistical analysis was performed by 2-tailed Student's *t* test or χ^2 test. A *P* value less than 0.05 was considered significant.

Study approval

Animal studies. All procedures performed on mice conformed to the ethical regulation guidelines of the Wellcome Trust Sanger Institute and to the guidelines of the UK Home Office (project license no. PPL80/2479).

Children. The ethical research committee of Kocaeli University Hospital approved the protocols (study no. 2013-1, site no. 12), and written consent was obtained from the adults accompanying the controls or patients.

Aged subjects. Clinical samples from aged subjects were from the previously described KIHD study (44).

Acknowledgments

The authors are grateful to the Sanger mouse facility for help with animal experiments; Kevin McKinzee for μCT data generation and analysis; Miep Helfrich for generous support; and Vasudev Kantae, Bhargavi Carasala, and Jonathan Broomfield for metabolite measurements. V.K. Yadav dedicates this study to his mother, Bhagwanti Devi. P. Roman-Garcia and I. Quiros-Gonzalez are supported by ERA-EDTA postdoctoral fellowships (ERA LTF-78/2011 and 107/2012). This work was supported by the Wellcome Trust (grant no. 098051).

Received for publication February 3, 2014, and accepted in revised form April 24, 2014.

Address correspondence to: Vijay K. Yadav, The Morgan Building (N235), Wellcome Trust Sanger Institute, Cambridge CB10 1SA, United Kingdom. Phone: 44.01223.496948; Fax: 44.01223.496826; E-mail: vy1@sanger.ac.uk.

1. Dloniak SM, French JA, Holekamp KE. Rank-related maternal effects of androgens on behaviour in wild spotted hyaenas. *Nature*. 2006;440(7088):1190–1193.
2. Oury F, et al. Maternal and offspring pools of osteocalcin influence brain development and functions. *Cell*. 2013;155(1):228–241.
3. Weaver IC, et al. Epigenetic programming by maternal behavior. *Nat Neurosci*. 2004;7(8):847–854.
4. Karsenty G, Kronenberg HM, Settembre C. Genetic control of bone formation. *Annu Rev Cell Dev Biol*. 2009;25:629–648.
5. Teitelbaum SL, Ross FP. Genetic regulation of osteoclast development and function. *Nat Rev Genet*. 2003;4(8):638–649.
6. Manolagas SC. Birth and death of bone cells: basic regulatory mechanisms and implications for the pathogenesis and treatment of osteoporosis. *Endocr Rev*. 2000;21(2):115–137.
7. Zaidi M. Skeletal remodeling in health and disease. *Nat Med*. 2007;13(7):791–801.
8. Khosla S. Pathogenesis of age-related bone loss in humans. *J Gerontol A Biol Sci Med Sci*. 2013; 68(10):1226–1235.
9. Harada S, Rodan GA. Control of osteoblast function and regulation of bone mass. *Nature*. 2003; 423(6937):349–355.
10. Goerss JB, Kim CH, Atkinson EJ, Eastell R, O'Fallon WM, Melton LJ. Risk of fractures in patients with pernicious anemia. *J Bone Miner Res*. 1992;7(5):573–579.
11. Dhonukshe-Rutten RA, van Dusseldorp M, Schneede J, de Groot LC, van Staveren WA. Low bone mineral density and bone mineral content are associated with low cobalamin status in adolescents. *Eur J Nutr*. 2005;44(6):341–347.
12. Tucker KL, et al. Low plasma vitamin B12 is associated with lower BMD: the Framingham Osteoporosis Study. *J Bone Miner Res*. 2005;20(1):152–158.
13. Morris MS, Jacques PF, Selhub J. Relation between homocysteine and B-vitamin status indicators and bone mineral density in older Americans. *Bone*. 2005;37(2):234–242.
14. Carmel R, Lau KH, Baylink DJ, Saxena S, Singer FR. Cobalamin and osteoblast-specific proteins. *N Engl J Med*. 1988;319(2):70–75.
15. Muthayya S, et al. Low maternal vitamin B12 status is associated with intrauterine growth retardation in urban South Indians. *Eur J Clin Nutr*. 2006; 60(6):791–801.

16. Merriman NA, Putt ME, Metz DC, Yang YX. Hip fracture risk in patients with a diagnosis of pernicious anemia. *Gastroenterology*. 2010;138(4):1330–1337.
17. Nielsen MJ, Rasmussen MR, Andersen CB, Nexo E, Moestrup SK. Vitamin B12 transport from food to the body's cells — a sophisticated, multistep pathway. *Nat Rev Gastroenterol Hepatol*. 2012;9(6):345–354.
18. Kalhan SC, Marczewski SE. Methionine, homocysteine, one carbon metabolism and fetal growth. *Rev Endocr Metab Disord*. 2012;13(2):109–119.
19. Lazar MA, Birnbaum MJ. Physiology. De-meaning of metabolism. *Science*. 2012;336(6089):1651–1652.
20. Stratikopoulos E, Szabolcs M, Dragatsis I, Klinakis A, Efstratiadis A. The hormonal action of IGF1 in postnatal mouse growth. *Proc Natl Acad Sci U S A*. 2008;105(49):19378–19383.
21. Long F, Joeng KS, Xuan S, Efstratiadis A, McMahon AP. Independent regulation of skeletal growth by Ihh and IGF signaling. *Dev Biol*. 2006;298(1):327–333.
22. Bex M, Bouillon R. Growth hormone and bone health. *Horm Res*. 2003;60(suppl 3):80–86.
23. DiGirolamo DJ, et al. Mode of growth hormone action in osteoblasts. *J Biol Chem*. 2007; 282(43):31666–31674.
24. Carroll PV, et al. Growth hormone deficiency in adulthood and the effects of growth hormone replacement: a review. Growth Hormone Research Society Scientific Committee. *J Clin Endocrinol Metab*. 1998;83(2):382–395.
25. Vijayakumar A, Yakar S, Leroith D. The intricate role of growth hormone in metabolism. *Front Endocrinol (Lausanne)*. 2011;2:32.
26. Lu M, et al. Insulin regulates liver metabolism in vivo in the absence of hepatic Akt and Foxo1. *Nat Med*. 2012;18(3):388–395.
27. Xian L, et al. Matrix IGF-1 maintains bone mass by activation of mTOR in mesenchymal stem cells. *Nat Med*. 2012;18(7):1095–1101.
28. Sturman JA. Taurine in development. *Physiol Rev*. 1993;73(1):119–147.
29. Verner A, Craig S, McGuire W. Effect of taurine supplementation on growth and development in preterm or low birth weight infants. *Cochrane Database Syst Rev*. 2007;(4):CD006072.
30. Herrington J, Smit LS, Schwartz J, Carter-Su C. The role of STAT proteins in growth hormone signaling. *Oncogene*. 2000;19(21):2585–2597.
31. Wan M, et al. Postprandial hepatic lipid metabolism requires signaling through Akt2 independent of the transcription factors FoxA2, FoxO1, and SREBP1c. *Cell Metab*. 2011;14(4):516–527.
32. Holloway MG, Cui Y, Laz EV, Hosui A, Hennighausen L, Waxman DJ. Loss of sexually dimorphic liver gene expression upon hepatocyte-specific deletion of Stat5a-Stat5b locus. *Endocrinology*. 2007; 148(5):1977–1986.
33. Fu Q, Yu X, Callaway CW, Lane RH, McKnight RA. Epigenetics: intrauterine growth retardation (IUGR) modifies the histone code along the rat hepatic IGF-1 gene. *FASEB J*. 2009;23(8):2438–2449.
34. Jing X, et al. Crosstalk of humoral and cell-cell contact-mediated signals in postnatal body growth. *Cell Rep*. 2012;2(3):652–665.
35. Masternak MM, Panici JA, Wang F, Wang Z, Spong A. The effects of growth hormone (GH) treatment on GH and insulin/IGF-1 signaling in long-lived Ames dwarf mice. *J Gerontol A Biol Sci Med Sci*. 2010; 65(1):24–30.
36. Sesmilo G, et al. Effects of growth hormone (GH) administration on homocyst(e)ine levels in men with GH deficiency: a randomized controlled trial. *J Clin Endocrinol Metab*. 2001;86(4):1518–1524.
37. Pons L, et al. Anchoring secreted proteins in endoplasmic reticulum by plant oleosin: the example of vitamin B12 cellular sequestration by transcobalamin. *PLoS One*. 2009;4(7):e6325.
38. Padmanabhan N, et al. Mutation in folate metabolism causes epigenetic instability and transgenerational effects on development. *Cell*. 2013;155(1):81–93.
39. Pettenuzzo LF, et al. Ascorbic acid prevents water maze behavioral deficits caused by early postnatal methylmalonic acid administration in the rat. *Brain Res*. 2003;976(2):234–242.
40. Schirra HJ, et al. Altered metabolism of growth hormone receptor mutant mice: a combined NMR metabonomics and microarray study. *PLoS One*. 2008;3(7):e2764.
41. Sun Z, Lazar MA. Dissociating fatty liver and diabetes. *Trends Endocrinol Metab*. 2013;24(1):4–12.
42. Yadav VK, et al. Pharmacological inhibition of gut-derived serotonin synthesis is a potential bone anabolic treatment for osteoporosis. *Nat Med*. 2010; 16(3):308–312.
43. Yadav VK, et al. Lrp5 controls bone formation by inhibiting serotonin synthesis in the duodenum. *Cell*. 2008;135(5):825–837.
44. Vanharanta M, Voutilainen S, Rissanen TH, Adlercreutz H, Salonen JT. Risk of cardiovascular disease-related and all-cause death according to serum concentrations of enterolactone: Kuopio Ischaemic Heart Disease Risk Factor Study. *Arch Intern Med*. 2003;163(9):1099–1104.
45. Stabler SP, Allen RH, Savage DG, Lindenbaum J. Clinical spectrum and diagnosis of cobalamin deficiency. *Blood*. 1990;76(5):871–881.